



Kashani, M. M., Barmi, A., & Malinova, V. (2015). Influence of inelastic buckling on low-cycle fatigue degradation of reinforcing bars. *Construction and Building Materials*, 94, 644–655. DOI: 10.1016/j.conbuildmat.2015.07.102

Peer reviewed version

Link to published version (if available):  
[10.1016/j.conbuildmat.2015.07.102](https://doi.org/10.1016/j.conbuildmat.2015.07.102)

[Link to publication record in Explore Bristol Research](#)  
PDF-document

## **University of Bristol - Explore Bristol Research**

### **General rights**

This document is made available in accordance with publisher policies. Please cite only the published version using the reference above. Full terms of use are available:  
<http://www.bristol.ac.uk/pure/about/ebr-terms.html>

# Influence of inelastic buckling on low-cycle fatigue degradation of reinforcing bars

Mohammad M. Kashani<sup>1</sup>, Aneeka K. Barmi<sup>2</sup>, Viktoria S. Malinova<sup>3</sup>

## Abstract

The effect of inelastic buckling on low-cycle high amplitude fatigue life of reinforcing bars is investigated experimentally. Ninety low-cycle fatigue tests on reinforcing bars varied in amplitudes and buckling lengths are conducted. Using scanning electron microscope the fractography of fractured surfaces are studied. The results show that the inelastic buckling, bar diameter and surface condition are the main parameters affecting the low-cycle fatigue life of reinforcing bars. Through nonlinear regression analyses of the experimental data a new set of empirical equations for fatigue life prediction of reinforcing bars as a function of the buckling length and yield strength are developed. Finally, these empirical models have been implemented into a new phenomenological hysteretic material model for reinforcing bars. The new material model is able to simulate the nonlinear stress-strain behaviour of reinforcing bars with the effect of inelastic buckling and low-cycle fatigue degradation. The results of simulation using the analytical model show a good agreement with the observed experimental results.

**Keywords:** Low-cycle fatigue, buckling, cyclic behaviour, reinforcing steel, stress-strain relation

---

<sup>1</sup>Lecturer, University of Bristol, Dept. of Civil Engineering University of Bristol, Bristol, BS8 1TR, United Kingdom (corresponding author), E-mail: mehdi.kashani@bristol.ac.uk

<sup>2</sup>MEng Student, University of Bristol, Dept. of Civil Engineering University of Bristol, Bristol, BS8 1TR, United Kingdom

<sup>3</sup>MEng Student, University of Bristol, Dept. of Civil Engineering University of Bristol, Bristol, BS8 1TR, United Kingdom

## 22 **1. Introduction**

23 The current performance-based seismic design philosophy of reinforced concrete (RC)  
24 structures relies on the proper detailing of plastic hinge regions where most of the inelastic  
25 deformations are expected to occur. The inelastic cyclic deformation in plastic hinge regions  
26 results in a significant tension and compression strain reversals. Among RC concrete  
27 components, RC bridges piers are the most vulnerable components. This is because the  
28 structural system of bridges is very simple (a single degree of freedom system). Unlike  
29 buildings where plastic hinges are designed to occur in beams, due to the nature of the  
30 structural system of bridges the plastic hinges are forced to occur in piers. As a result, they  
31 should be able to accommodate a significant inelastic deformation due to earthquake loading.  
32 Therefore, several researchers have studied the nonlinear behaviour of RC components under  
33 cyclic loading [1,2]. In these studies fracture of vertical reinforcing bars in RC columns under  
34 cyclic loading has been observed [1,2] which is due to the low-cycle high amplitude fatigue  
35 degradation of vertical reinforcing bars.

36 Moreover, there is a large number of existing bridges around the world that were designed  
37 prior to the modern seismic design codes and therefore they are not properly detailed for  
38 seismic loading. One of the most common type of failure mode of RC bridge piers that has  
39 been observed in real earthquakes and experimental testing is the buckling of vertical  
40 reinforcement which is then followed by fracture of reinforcement in tension due to low-  
41 cycle high amplitude fatigue degradation [1,2,3]. Therefore, several researchers have  
42 investigated the nonlinear cyclic behaviour of reinforcing bars with the effect of inelastic  
43 buckling [4-12]. The experimental results showed that the inelastic buckling has a great  
44 influence on low-cycle fatigue life of reinforcing bars. More recently Kashani [13]  
45 investigated the nonlinear behaviour of RC bridge piers numerically and compared with the  
46 experimental data reported in [1,2]. They have reported that the buckling length of

47 longitudinal reinforcing bars in RC columns has a significant impact of the fracture of these  
48 bars in tension. However, despite the previous research in this area, there has not been any  
49 experimental study to explore and quantify the significance of inelastic buckling on low-cycle  
50 fatigue life of reinforcing bars.

51 This paper is addressing this issue and explores the impact of inelastic buckling on low-cycle  
52 fatigue life of reinforcing bars. Therefore, a comprehensive experimental testing conducted  
53 on ninety reinforcing bars under low-cycle fatigue strain history varied in buckling lengths  
54 (slenderness ratio), diameters, yield strengths and surface roughness (ribbed and smooth  
55 bars). Using the scanning electron microscope (SEM) a fractography analysis of the fractured  
56 surfaces are conducted. Finally, using the experimental results a set of empirical models are  
57 developed to predict the low-cycle fatigue life of reinforcing bars as a function of buckling  
58 length and yield strength.

59 Moreover, earlier research by Kashani [13] resulted in development of a new  
60 phenomenological hysteretic material model for reinforcing bars which is implemented in the  
61 OpenSees [14] an open source finite element code for nonlinear seismic analysis of  
62 structures. This model is capable of simulating the nonlinear cyclic behaviour of reinforcing  
63 bars with the effect of inelastic buckling and low-cycle fatigue degradation. However, due to  
64 the paucity of experimental data in the literature, the fatigue material parameters have not  
65 been calibrated to account for the influence of buckling on low-cycle fatigue degradation of  
66 reinforcing bars. The experimental data and empirical models in this paper helped to improve  
67 this feature of Kashani's model. The results of the improved analytical model are in a good  
68 agreement with the observed experimental results. Moreover, this model is readily available  
69 in the OpenSees to be used by the earthquake engineering community for nonlinear seismic  
70 analysis of RC bridges/structures.

71

## 2. Experimental programme

A total of ninety test specimens are prepared for low-cycle high amplitude fatigue tests. The reinforcement used in this experiment are B500B ribbed and B460 smooth British manufactured reinforcing bars [15]. The specimens are including thirty 12mm diameter ribbed reinforcing bars, thirty 16mm diameter ribbed reinforcing bars and thirty 12mm diameter smooth reinforcing bars. For each group of test specimens three tension tests are conducted to evaluate the material properties. Table 1 summarises the material properties of test specimens and Fig. 1 shows the typical stress-strain curve for each group of test specimens.

**Table 1 Mechanical properties of tests specimens**

		<b>16mm Ribbed</b>	<b>12mm Ribbed</b>	<b>12mm Smooth</b>
Yield strain	$\varepsilon_y$	0.0027	0.0028	0.0023
Yield stress (MPa)	$\sigma_y$	535.67	544.33	474.5
Elastic modulus (MPa)	$E_s$	200000	191666.67	204500
Hardening strain	$\varepsilon_{sh}$	0.0183	0.0287	0.0046
Strain at maximum stress	$\varepsilon_u$	0.104	0.143	0.061
Maximum stress (MPa)	$\sigma_u$	633.75	640.67	510.564
Fracture strain	$\varepsilon_r$	0.195	0.222	0.54185

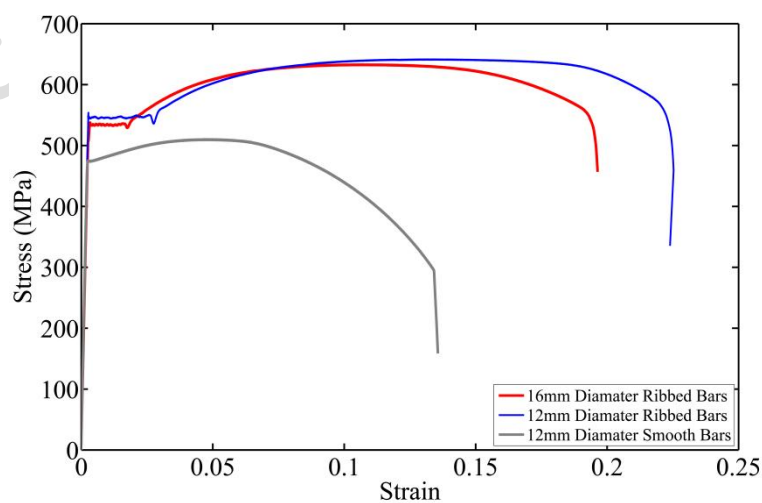


**Fig. 1. Stress-strain behaviour of test specimens in tension**

## 86 2.1. Low-cycle high amplitude fatigue test

87 A total of ninety low-cycle fatigue tests are conducted on reinforcing bars with different  
88 buckling lengths and strain amplitudes. It is well known that the buckling length of the  
89 vertical reinforcing bars inside RC columns is a function of the stiffness of horizontal tie  
90 reinforcement [13]. Therefore, slenderness ratios for the experiment are chosen based on the  
91 common observed buckling modes of vertical reinforcement in RC columns as report in [13].  
92 The slenderness ratio is defined by the  $L/D$  ratio where  $L$  is the length and  $D$  is the bar  
93 diameter. The  $L/D$  ratios tested in this experiment are 5, 8, 10, 12 and 15.

94 A 250kN universal testing machine with hydraulic grips was used for the low-cycle fatigue  
95 testing of the reinforcing bars. The machine used an integral Linear Variable Displacement  
96 Transducer (LVDT) to measure the displacement of the grips. A displacement control loading  
97 protocol with zero mean strain using a sine wave loading pattern with constant amplitude is  
98 used in the low-cycle fatigue tests. The strain rate is set to 0.005strain/sec throughout the  
99 experiment. The total strain amplitudes used in the low-cycle fatigue tests are 1%, 1.5% 2%,  
100 3%, 4% and 5% for 12mm diameter bars and 1%, 1.5% 2%, 2.5% 3% and 4% for 16mm  
101 diameter bars. A picture of the three groups of bars used in the low-cycle fatigue tests is  
102 shown in Fig. 2. It should be noted that the failure of the specimen is taken to be the point at  
103 which the bar is completely fractured.

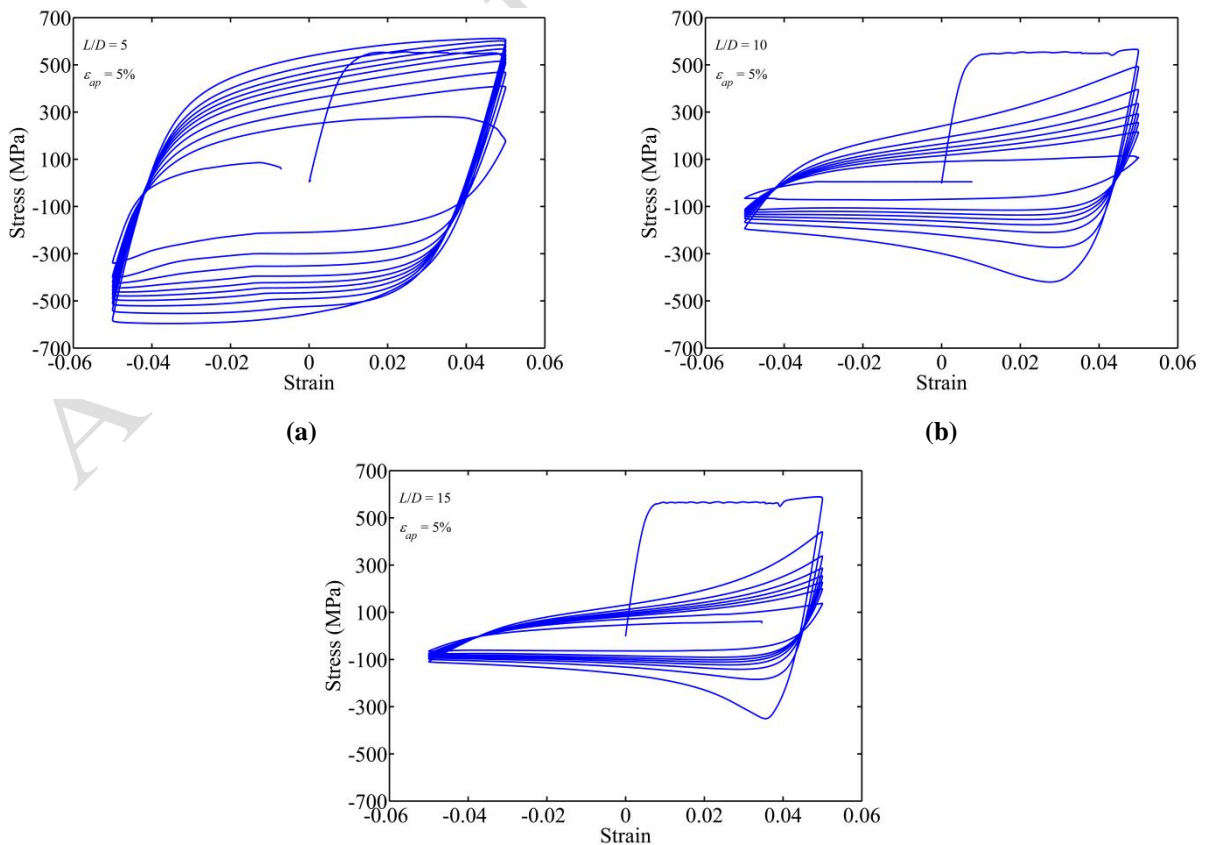


104  
105 **Fig. 2. Low-cycle fatigue test specimens**

106 **3. Experimental results and discussion**

107 **3.1. Influence of inelastic buckling and slenderness ratio**

108 Fig. 3 shows an example hysteretic response of 12mm ribbed bars under low-cycle fatigue  
109 test at 5% strain amplitude. Fig. 3 (a) shows that hysteretic response of the bars with  $L/D = 5$   
110 are almost symmetrical in tension and compression. However, as the slenderness ratio of bars  
111 increases a pinching response is observed which is due to the impact of inelastic buckling and  
112 geometrical nonlinearity on the hysteretic response. The results show that the fatigue induced  
113 crack initiation in the group of bars with  $L/D = 10$  and  $15$  is much quicker than the group of  
114 bars with  $L/D = 5$ . Moreover, It was observed that crack always started at the inside face of  
115 the buckle bar. This is because, when a bar buckles the total strain amplitude at inside face of  
116 the bar increases due to the combined axial and bending deformation which is known as  
117 second order effect. Therefore, the low-cycle fatigue has a more severe effect in bars with  
118 larger  $L/D$  ratio. Fig. 4 shows an example of fractured bars after low-cycle fatigue test.



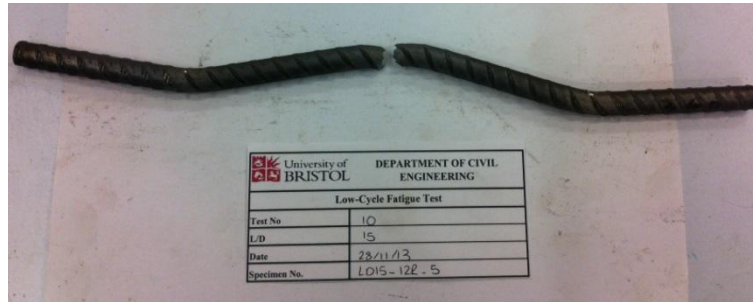
119  
120

121

122  
123

(a)

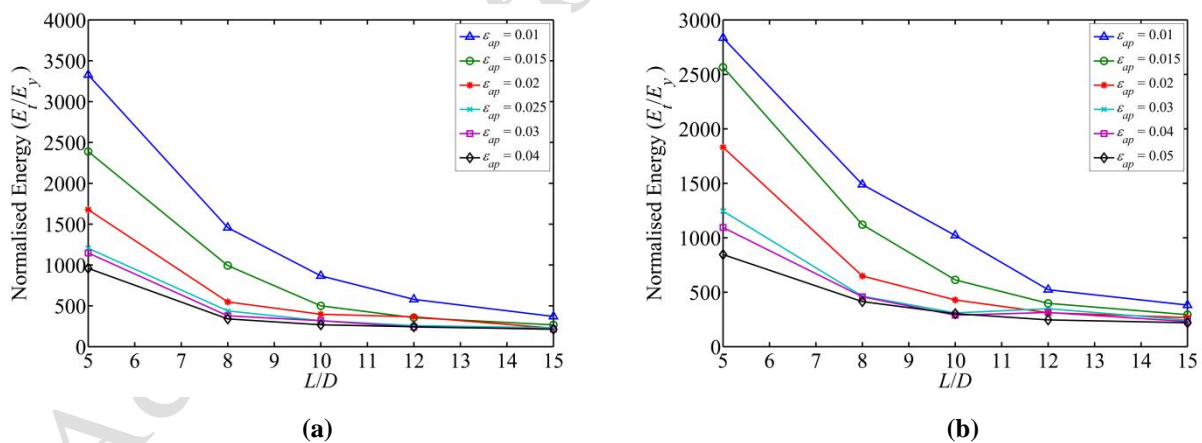
Fig. 3. Hysteretic response of 12mm ribbed reinforcing bars: (a)  $L/D = 5$ , (b)  $L/D = 10$ , (c)  $L/D = 15$



124  
125

Fig. 4. Buckled shape of a 12mm diameter bar with  $L/D = 15$  after failure

126 In order to show the impact of buckling on low-cycle fatigue degradation of reinforcing bars  
127 a comparison is made between the total energy dissipation and cyclic stress degradation of  
128 different groups of bars. Fig. 5 shows the normalised total hysteretic energy for ribbed bars  
129 with 12mm and 16mm diameter and varied in slenderness ratios and strain amplitudes. The  
130 variable  $E_t$  is the total hysteretic energy of bars in low-cycle fatigue test and  $E_y$  is the elastic  
131 energy of the corresponding bars under monotonic tension.



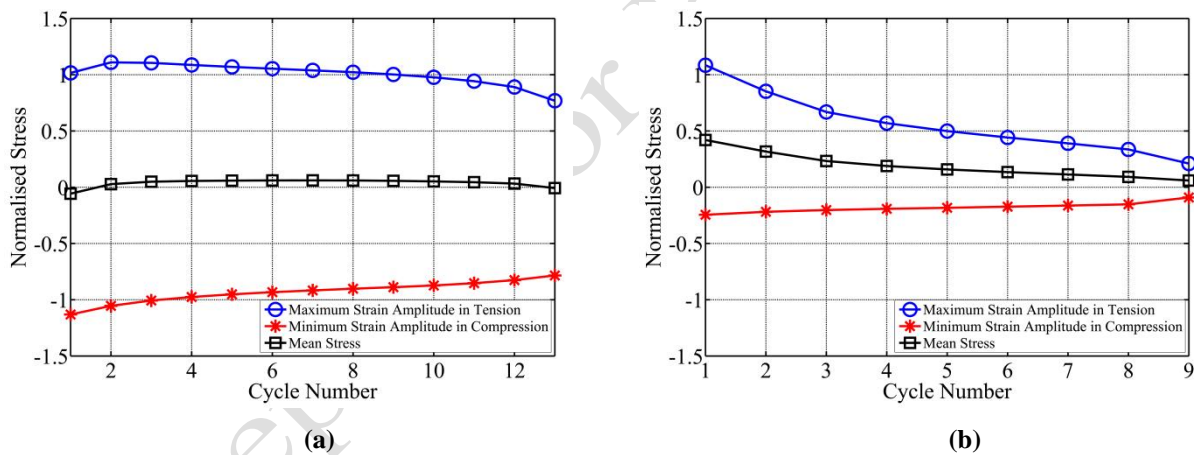
132  
133  
134

Fig. 5. Normalised dissipated hysteretic energy: (a) 16mm ribbed bars (b) 12mm ribbed bars

135 As it is shown in Fig. 5, buckling has a more significant impact on energy dissipation at  
136 lower strain amplitude. As the strain amplitude increases beyond 2.5% almost all of the bars  
137 with  $L/D \geq 8$  converge towards the same point.



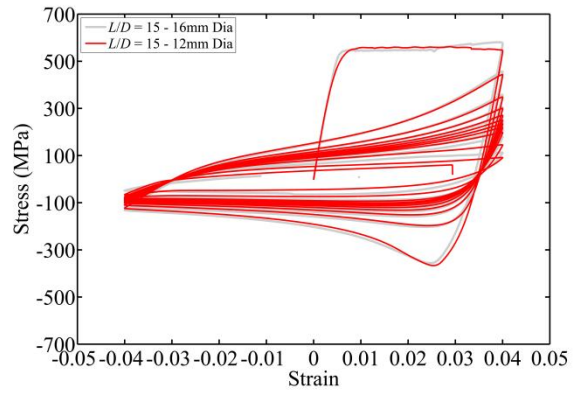
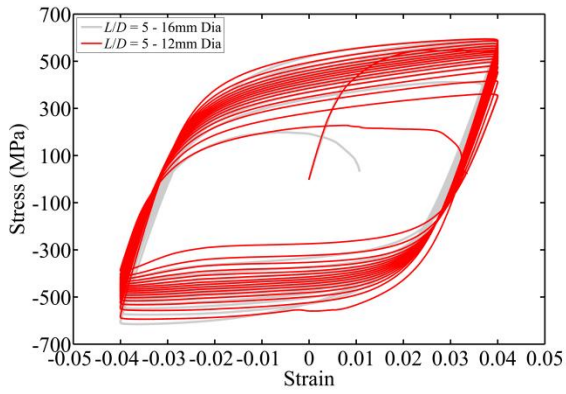
138 Fig. 6 shows example graphs of the cyclic stress loss of 16mm diameter bars under low-cycle  
 139 fatigue test with 4% strain amplitude. It should be noted that the normalised stress in Fig. 6 is  
 140 the value of the stress at the pick strain amplitude in tension and compression in each half  
 141 cycle normalised to the yield stress. Fig. 6 (a) shows that the stress loss in tension and  
 142 compression is almost symmetrical for bars with  $L/D = 5$ . Given a zero mean strain history is  
 143 used in the experiment, as expected, the mean stress loss is almost zero in bars with  $L/D = 5$ .  
 144 However, as it is shown in Fig. 6 (b) the normalised stress loss in tension and compression is  
 145 not symmetrical for bars with  $L/D = 15$ . This results in moving the normalised mean stress  
 146 graph from zero. This indicates that buckling increases the stress loss of reinforcing bars in  
 147 compression under cycling loading. Moreover, Fig. 6 (b) shows that the stress loss in tension  
 148 much faster than bars with  $L/D = 5$ .



149  
 150 (a) (b)  
 151 Fig. 6. Stress degradation of 16mm ribbed bars: (a)  $L/D = 5$ , 4% strain amplitude (b)  $L/D = 15$ , 4% strain  
 152 amplitude

### 153 3.2. Influence of bar diameter

154 The observed hysteretic responses of 12mm and 16mm diameter bars with  $L/D = 5$  and 15 are  
 155 shown in Fig. 7. It is clear that the diameter does not have a significant impact of hysteric  
 156 response and buckling behaviour of reinforcing bars.



157

158

159

160

161

162

163

164

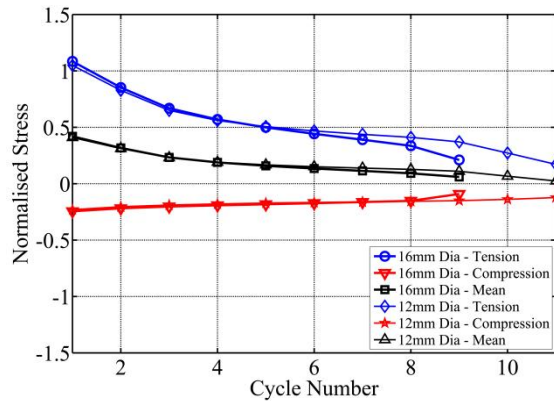
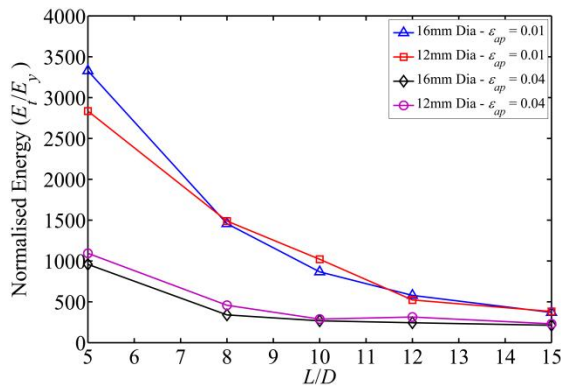
165

(a)

(b)

**Fig. 7. Hysteretic response of reinforcing bars with different diameter and slenderness ratio: (a)  $L/D = 5$ , 12mm and 16mm Dia (b)  $L/D = 15$ , 12mm and 16mm Dia**

Furthermore, Fig. 8(a) shows that the diameter has a very small impact on the total dissipated hysteretic energy. However, Fig. 8(b) shows that although the stress degradation trend is almost the same in 12mm and 16mm diameter bars, the 16mm diameter bars have a shorter fatigue life compare to 12mm diameter bars. This suggests that the larger diameter bars have shorter low-cycle fatigue life.



166

167

168

169

170

171

172

173

174

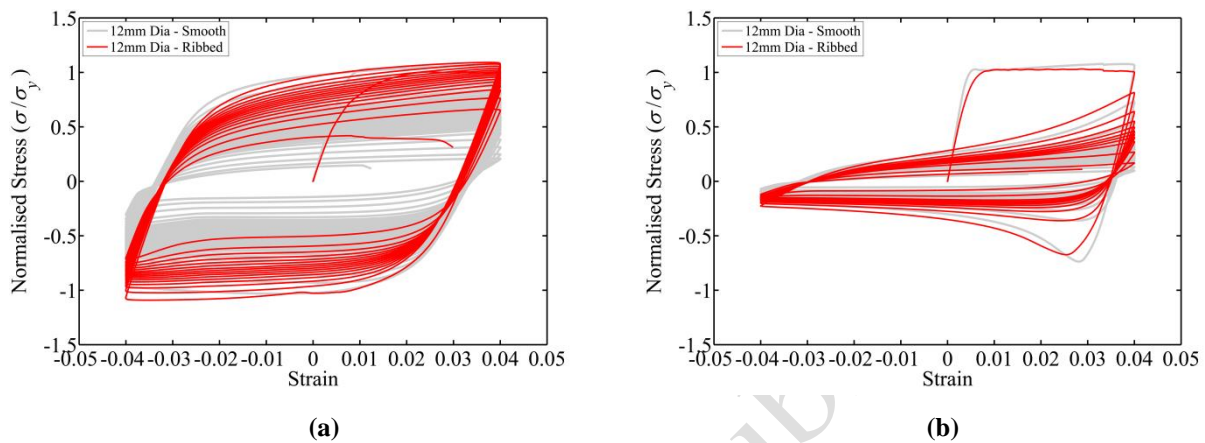
(a)

(b)

**Fig. 8. Influence of bar diameter on cyclic degradation: (a) Hysteretic energy dissipation and (b) stress degradation ( $L/D = 15$  at 4% strain amplitude)**

### 175 3.3. Influence of material type and surface condition

176 Fig. 9 shows a comparison between the hysteretic responses of 12mm diameter ribbed and  
177 smooth bars. Given the yield stress ( $\sigma_y$ ) is different in these bars, the stress ( $\sigma$ ) is normalised  
178 to their corresponding yield stress.

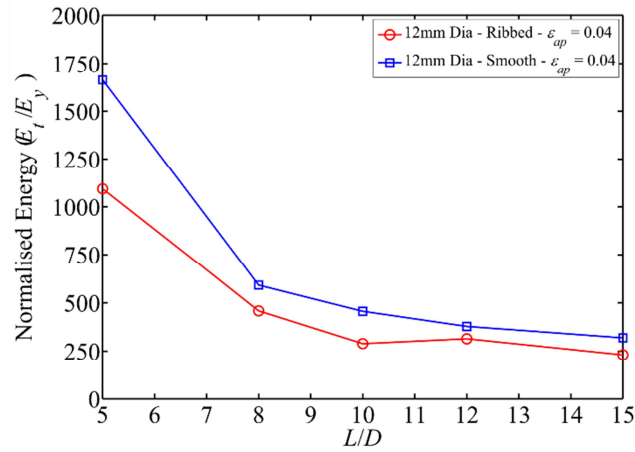


179

180

181 **Fig. 9. Hysteretic response of smooth and ribbed bars with 12mm in diameter: (a)  $L/D = 5$  (b)  $L/D = 15$**

182 The observed responses in Fig. 9(a) shows that the cyclic stress degradation is much higher in  
183 smooth bars compare to ribbed bars in  $L/D = 5$ . However, Fig. 9(b) shows that the stress  
184 degradation difference between the smooth and ribbed bars is much lower in bars with  $L/D =$   
185 15. Despite the high degradation rate in smooth bars, it is found that the fatigue life of the  
186 smooth bars is higher than ribbed bars and their failure mode is more ductile compare to  
187 ribbed bars. As slenderness ratio of bars increased the difference in the fatigue life of ribbed  
188 and smooth bars became much smaller which is due to the impact of buckling on the low-  
189 cycle fatigue life of bars. Fig. 10 shows the total energy loss of 12mm diameter ribbed and  
190 smooth reinforcing bars under 4% strain amplitude and varied  $L/D$  ratios.



191  
192

**Fig. 10. Comparison of the hysteretic energy dissipation in smooth and ribbed bars**

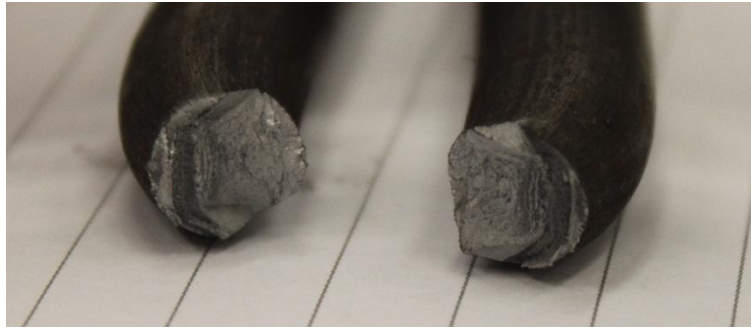
193 Despite the lower ductility (area under stress-strain curve in tension) of smooth bars in  
 194 monotonic tension they showed more ductile behaviour under cyclic loading (area inside the  
 195 cyclic stress-strain curve). This is primarily due to the surface conditions as reported by other  
 196 researchers [16-19]. [16] reported that the fatigue life of ribbed bars is generally lower than  
 197 smooth bars due to the stress concentration at the root of the ribs which results in crack  
 198 initiation at these locations. Therefore, the failure mode is less ductile compare to smooth  
 199 bars. Fig. 11 shows examples of fractured surfaces of ribbed and smooth bars. Further  
 200 discussion about the fractured surfaces is available in section 3.4 of this paper.

201 It can be concluded from Fig. 10 that the surface roughness has a great influence on the  
 202 fatigue life of reinforcing bars with small  $L/D$  ratio. However, as the  $L/D$  ratio increases the  
 203 impact of buckling is more severe than the surface roughness and therefore the inelastic  
 204 buckling has a greater influence on the low-cycle fatigue life of reinforcing bars.



205  
206

(a)



(b)

**Fig. 11. Observed fracture surface of 12mm diameter bars after low-cycle fatigue test with 5% strain amplitude: (a) a ribbed bar with  $L/D = 15$  and (b) a smooth bar with  $L/D = 15$**

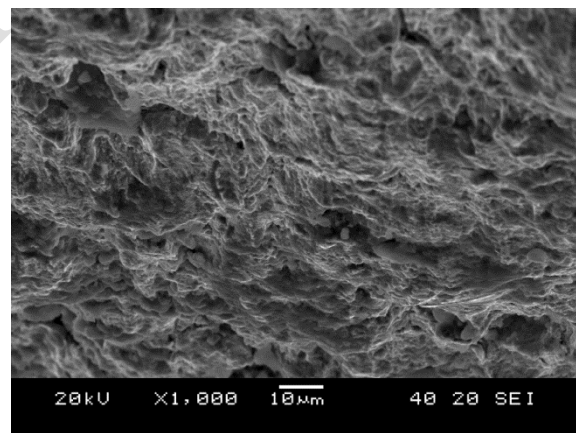
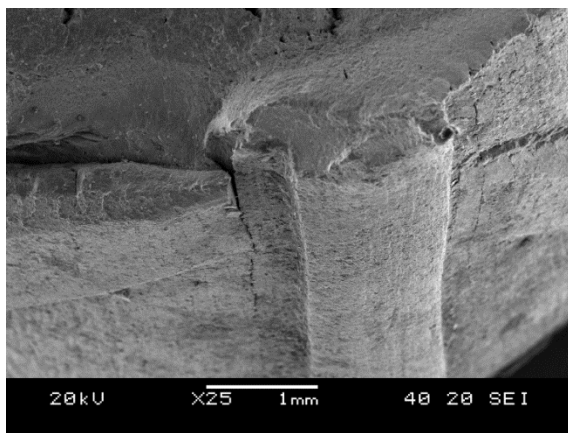
### **3.4. Fractography of the fractured surfaces using Scanning Electron Microscope (SEM)**

SEM was used for fractography of the fractured surfaces. This was used to take detailed images of some sample fractured specimens to investigate the crack propagation by topography of the fractured surface. This apparatus focusses a beam of high energy electrons on to the specimens that interact with the atoms at the surface to produce a detailed scan of the specimen.

As explained in section 3.3, The fatigue crack of the ribbed bars under repeated cyclic loading initiated along the root of the transverse rib on the inside face of the buckled bar. After initiation, the cracks propagated away from the transverse rib on the bar surface into the body of the bar normal to the bar axis. This suggests that the largest stresses lie in the longitudinal direction, as otherwise the cracks would have grown along the along the root where the magnitudes of stress concentrations are much higher than elsewhere. The fatigue crack of the smooth bars also initiated on the inside face of the buckled bar and propagated away from the bar surface into the body of the bar normal to the bar axis. However, the crack initiation and propagation of smooth bars were much slower than ribbed bars. This difference

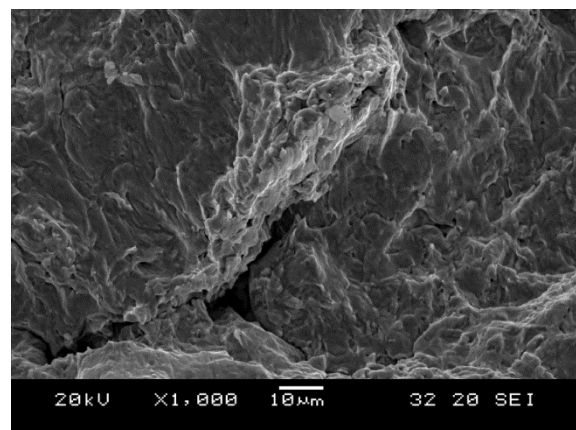
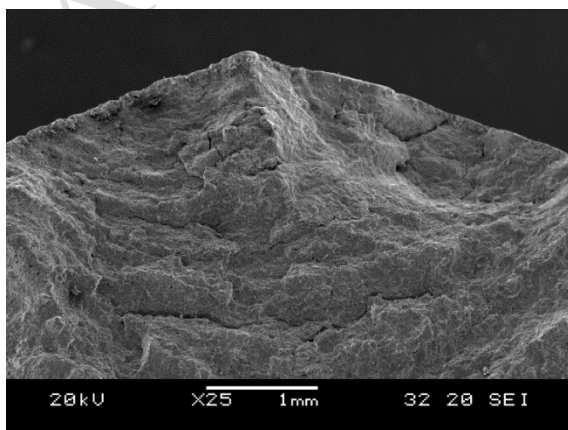
227 in the behaviour resulted in more ductile failure of smooth bars compare to ribbed bars with  
228 the same  $L/D$  ratio and strain amplitude.

229 Fig. 12 (a-f) shows the fractographs of 12mm ribbed and smooth bars and 16mm ribbed bars  
230 with  $L/D = 15$ . Comparing Fig. 12(a) and (b) with Fig. 12(c) and (d) shows that the dark areas  
231 of striation are associated with slower crack propagation in smooth bars (Fig. 12(c) and (d))  
232 that took longer to fracture and showed more plastic deformation. The lighter areas in ribbed  
233 specimens shows a more sudden fracture near the rib root as shown in Fig. 12(a) and (b) and  
234 Fig. 12(e) and (f). Moreover, the fracture surface of 16mm diameter ribbed bars in Fig. 12(e)  
235 and (f) shows lighter areas than 12mm diameter ribbed bars. This indicates that the diameter  
236 of bars increases the facture of bars become less ductile. The discussion of the influence of  
237 bar diameter on low-cycle fatigue life of reinforcing bars requires further experimental testing  
238 and is an area for future research.



239  
240 (a)

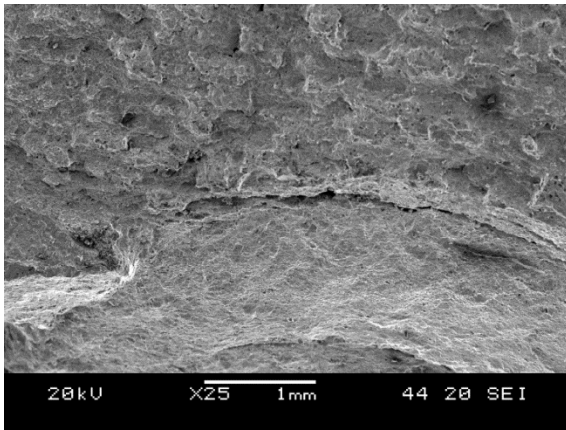
(b)



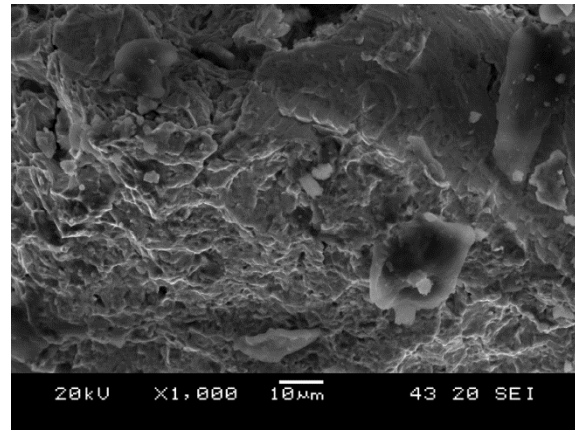
241

242

(c)



(d)



243

244

(e)

(f)

245

**Fig. 12. SEM fractographs of fractured bars with  $L/D = 15$  after low cycle fatigue tests at 4% strain**

246

**amplitude: (a) and (b) 12mm diameter ribbed bars (c) and (d) 12mm diameter smooth bars (e) and (f)**

247

**16mm diameter ribbed bars**

248

#### **4. Modelling low-cycle fatigue life of reinforcing bars**

249

##### **4.1. Basic low-cycle fatigue model using strain life approach**

250

The low-cycle fatigue life of reinforcing bars without the effect of buckling has been studied

251

by several researchers [3,16,17,19]. They have mainly used three methods to model the low-

252

cycle fatigue life of reinforcing bars i.e. Coffin-Manson [20], Koh-Stephen [21] and energy

253

method [22]. It should be noted that these models are only valid for low-cycle fatigue under

254

constant amplitude loading. Therefore, Miner's rule [23] can be employed to account for the

255

cumulative damage due to random loading history (further discussion is available in [3,5,7]).

256

Among the aforementioned models, Coffin-Manson and Koh-Stephen are more popular

257

among researchers as they are easy to be implemented to any finite element package for

258

seismic analysis of civil engineering structures such as OpenSees [14].

259

Both Coffin-Manson and Koh-Stephen models are using strain life approach to model the

260

low-cycle fatigue life of engineering materials. The plastic strain amplitude is the most

261

important parameter affecting the low-cycle fatigue life of material. Therefore, Coffin-

262 Manson model, as described in Eq. (1), relates the plastic strain amplitude ( $\varepsilon_p$ ) to the fatigue  
 263 life.

$$264 \quad \varepsilon_p = \varepsilon'_f (2N_f)^c \quad (1)$$

265 where,  $\varepsilon'_f$  is the ductility coefficient i.e. the plastic fracture strain for a single load reversal,  $c$   
 266 is the ductility exponent and  $2N_f$  is the number of half-cycles (load reversals) to failure.

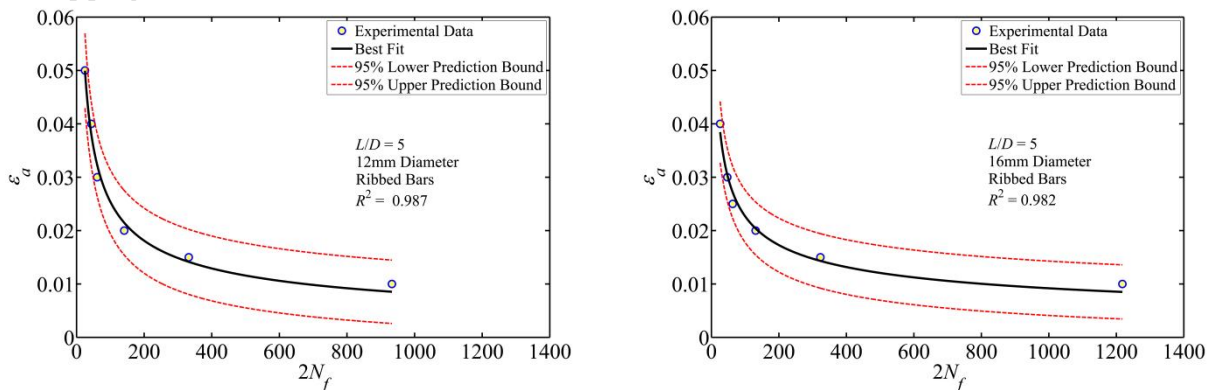
267 Koh-Stephen [21] extended the Coffin-Manson [20] for modelling the low-cycle fatigue life  
 268 of materials based on the total strain amplitude (elastic strain + plastic strain) as described in  
 269 Eq. (2).

$$270 \quad \varepsilon_a = \varepsilon_f (2N_f)^\alpha \quad (2)$$

271 where,  $\varepsilon_f$  is the ductility coefficient i.e. the total fracture strain for a single load reversal,  $\alpha$  is  
 272 the ductility exponent and  $2N_f$  is the number of half-cycles (load reversals) to failure.

273 In this research, the Koh-Stephen model is used to predict the low-cycle fatigue life of  
 274 reinforcing bars. Furthermore, the influence of inelastic buckling on fatigue material  
 275 constants  $\varepsilon_f$  and  $\alpha$  is also explored.

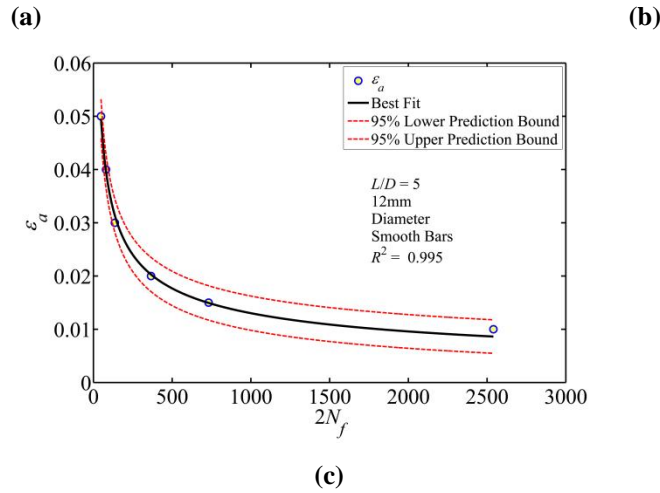
276 Eq. (2) is fitted to the observed experimental data of each slenderness ratio individually to  
 277 calibrate the fatigue material constants ( $\varepsilon_f$  and  $\alpha$ ). The results of the regression analyses are  
 278 summarised in Table 2. Fig. 13 shows example of the Eq. (2) fitted to the experimental data  
 279 for three groups of bars using a nonlinear regression analysis.



280



281



282

283

284 **Fig. 13. Calibration of the fatigue material constant for reinforcing bars with  $L/D = 5$ : (a) 12mm diameter**  
 285 **ribbed bars (b) 16mm diameter ribbed bars (c) 12mm diameter smooth bars**

286

**Table 2 Results of regression analysis to calibrate the low-cycle fatigue material constants**

12mm Ribbed Bars				16mm Ribbed Bars				12mm Smooth Bars			
$L/D$	$\epsilon_f$	$\alpha$	$R^2$	$L/D$	$\epsilon_f$	$\alpha$	$R^2$	$L/D$	$\epsilon_f$	$\alpha$	$R^2$
5	0.188	-0.448	0.987	5	0.138	-0.393	0.982	5	0.245	-0.491	0.996
8	0.262	-0.608	0.963	8	0.128	-0.470	0.981	8	0.228	-0.565	0.999
10	0.279	-0.660	0.942	10	0.192	-0.602	0.990	10	0.355	-0.715	0.995
12	0.398	-0.734	0.907	12	0.254	-0.677	0.962	12	0.457	-0.772	0.994
15	0.484	-0.799	0.983	15	0.407	-0.810	0.987	15	0.734	-0.907	0.996

287

#### 288 4.2. Correlation between the fatigue material constants and inelastic buckling

289 The inelastic buckling behaviour of reinforcing bars has been investigated by several  
 290 researchers [4,8,11,6,7,24]. In all of the previous studies researchers have agreed that the  
 291 post-buckling behaviour of reinforcing bars is affected by yield stress  $\sigma_y$  and geometrical  
 292 slenderness ratio  $L/D$ . Dhakal-Maekawa [11] found that the post buckling behaviour of  
 293 reinforcing bars is govern by a single compound variable called non-dimensional bar  
 294 buckling parameter  $\lambda_p$  as described in Eq. (3).

$$295 \lambda_p = \sqrt{\frac{\sigma_y}{100} \frac{L}{D}} \quad (3)$$

296 Where,  $\sigma_y$  is the yield stress and  $L/D$  is the geometrical slenderness ratio of reinforcing bars.

297 It should be noted that the yield stress in Eq. (3) should be in MPa.

298 Kashani [13] developed a new phenomenological hysteretic model for reinforcing bars that  
 299 accounts for inelastic buckling and low-cycle fatigue degradation. This model uses the  $\lambda_p$  to  
 300 define the post-buckling and cyclic response of reinforcing bars. However, the influence of  
 301 inelastic buckling on the low-cycle fatigue degradation is not currently included in the model.  
 302 Therefore, in this section the correlation between  $\lambda_p$  and low-cycle fatigue material constants  
 303 is explored. Further discussion about this model is available in section 5 of this paper.  
 304 In this study the Pearson's linear correlation coefficient ( $\rho$ ) is employed to investigate the  
 305 correlation of the  $\lambda_p$  and the low-cycle fatigue material constants  $\alpha$  and  $\varepsilon_f$ . The calculated  
 306 correlation coefficients together with P-values at 0.05 significance are shown in Table 3.

307 **Table 3 Correlation between the fatigue material constants and  $\lambda_p$**

Model Parameter	16mm Ribbed		12mm Ribbed		12mm Smooth	
	$\alpha$	$\varepsilon_p$	$\alpha$	$\varepsilon_p$	$\alpha$	$\varepsilon_p$
<b>Pearson</b>						
$\rho$	-0.9924	0.9191	-0.9618	0.9887	-0.9569	0.9881
<b>P-value</b>	$7.90 \times 10^{-4}$	0.0273	0.0089	0.0014	0.0107	0.0016

308  
 309 The results of correlation analysis show that there is a very strong negative correlation  
 310 between  $\alpha$  and  $\lambda_p$  and there is a very strong positive correlation between  $\varepsilon_f$  and  $\lambda_p$ . This is also  
 311 clear from the corresponding P-values of the fatigue material constants  $\alpha$  and  $\varepsilon_f$  which are all  
 312 less than the considered significance level (0.05). This shows that the dependence of the  
 313 fatigue material constants and  $\lambda_p$  is statistically significant. The interrelationship between the  
 314 fatigue material constants and the  $\lambda_p$  is modelled using regression analysis of the data. The  
 315 results of the regression analysis are shown in Fig. 14 (a-f).

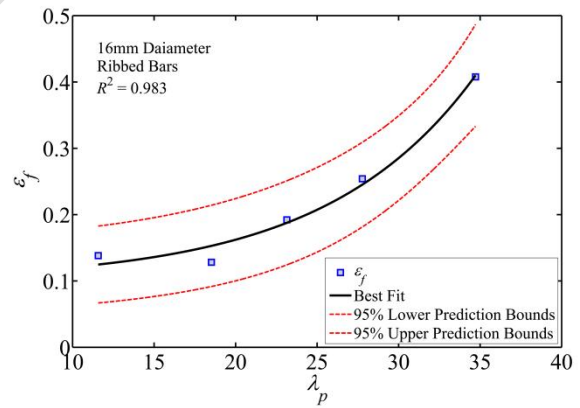
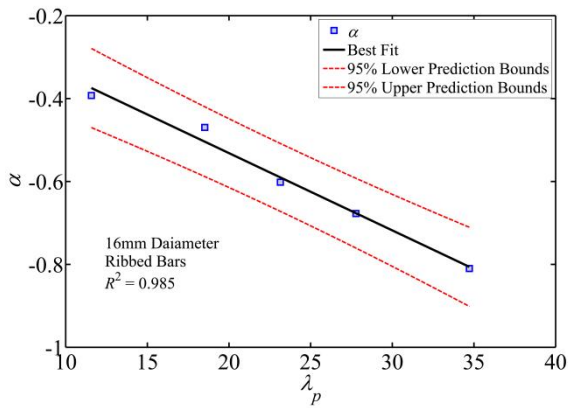
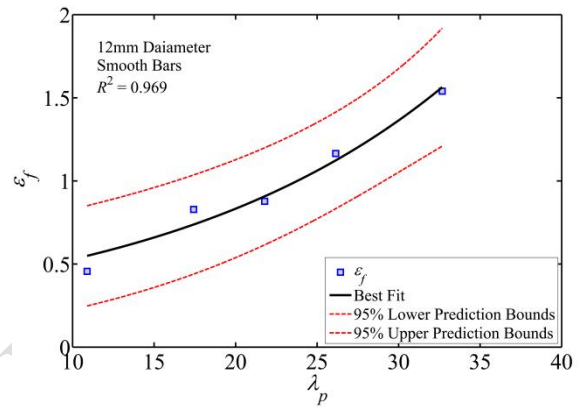
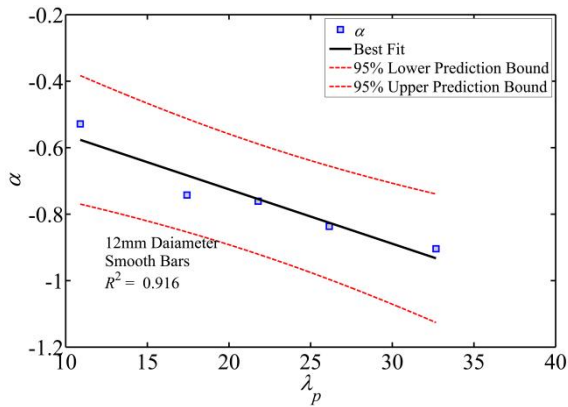
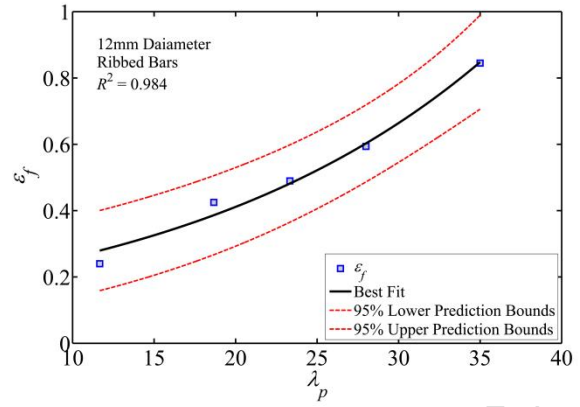
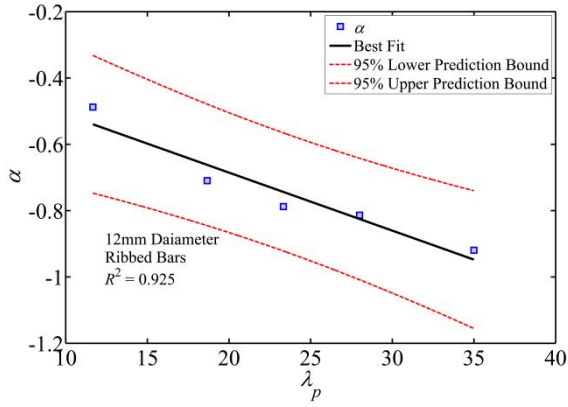


**Fig. 14. Influence of non-dimensional slenderness ratio on fatigue material constants: (a), (c), (e) Impact of buckling on  $\alpha$  and (b), (d), (f) Impact of buckling on  $\epsilon_f$**

The relationship between the fatigue model parameters and  $\lambda_p$  is defined by empirical Eq. (4) and (5) which are the results of the regression analysis shown in Fig 14.

$$\alpha = a \lambda_p - b \quad (4)$$

327  $\varepsilon_f = c \exp(d \lambda_p) + e$  (5)

328 where,  $\alpha$  and  $\varepsilon_f$  are the fatigue material constants,  $a$ ,  $b$ ,  $c$ ,  $d$  and  $e$  are the regression  
 329 coefficients that are shown in Table 4.

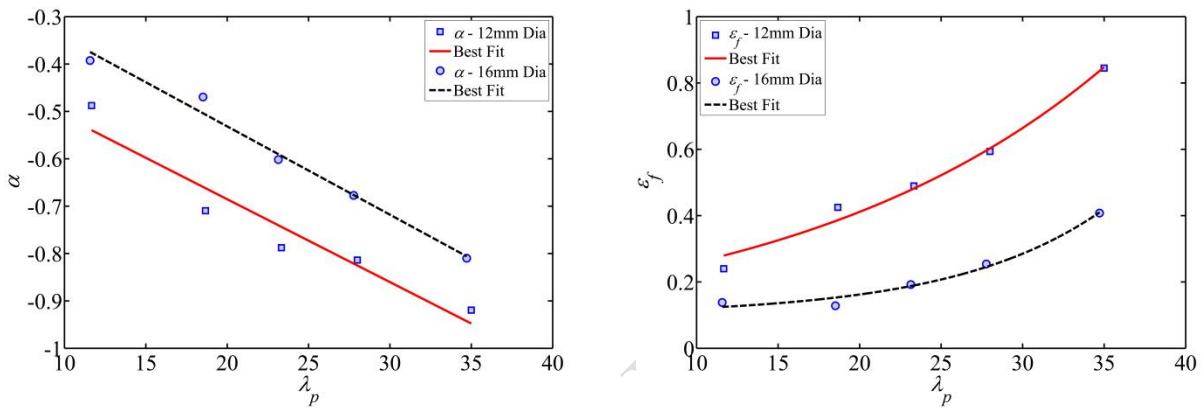
330 **Table 4 The proposed fatigue material constants as a function of the  $\lambda_p$**

Material constants	$a$	$b$	$c$	$d$	$e$
<b>12mm Dia ribbed bars</b>					
$\alpha$	-0.015	0.304			
$\varepsilon_f$			0.100	0.045	0.030
<b>16mm Dia ribbed bars</b>					
$\alpha$	0.018	0.159			
$\varepsilon_f$			0.007	0.109	0.100
<b>12mm Dia smooth bars</b>					
$\alpha$	-0.013	0.378			
$\varepsilon_f$			0.040	0.079	0.300

342  
 343 The results of regression analysis show that regardless of the reinforcement type (smooth or  
 344 ribbed bars) by increasing the  $\lambda_p$  the ductility coefficient  $\varepsilon_f$  increases exponentially but  
 345 ductility exponent  $\alpha$  decreases linearly. The reduction in ductility exponent ( $\alpha$ ) is due to the  
 346 increase in strain amplitude locally at the location of the plastic hinge in the bar due to  
 347 buckling. This will result in premature crack initiation in bars with bigger  $\lambda_p$ . However,  
 348 increasing the ductility coefficient ( $\varepsilon_f$ ) means that the fracture strain of bar under once cycle  
 349 increases by increasing the  $\lambda_p$ . The hysteretic response of bars previously shown in Fig. 3  
 350 indicates that the bars with bigger slenderness ratio after buckling in compression are not able  
 351 to recover the stress in tension after load reversal with the same strain amplitude in tension.  
 352 This is due the influence of geometrical nonlinearity and significant residual plastic  
 353 deformation in compression. This indicates that mean strain has a big influence on the low-  
 354 cycle fatigue life of reinforcing bars. The combined influence of inelastic buckling and mean  
 355 strain is out of the scope of this paper and is an area for future.

356 Another important finding in this research is the influence of bar diameter on fatigue material  
 357 constants. Fig. 15 shows a comparison between the fatigue material constants of 12mm and

358 16mm diameter ribbed bars as a function of  $\lambda_p$ . As expected the 16mm diameter bars have  
 359 smaller low-cycle fatigue life compare to 12mm diameter bars. These results are in a good  
 360 agreement with results observed by other researchers [3,16]. However, the influence of bar  
 361 diameter increases by increasing the  $\lambda_p$ . This indicates that there is need for further study to  
 362 explore the impact of bar diameter on low-cycle fatigue life of reinforcing bars with the effect  
 363 of inelastic buckling.



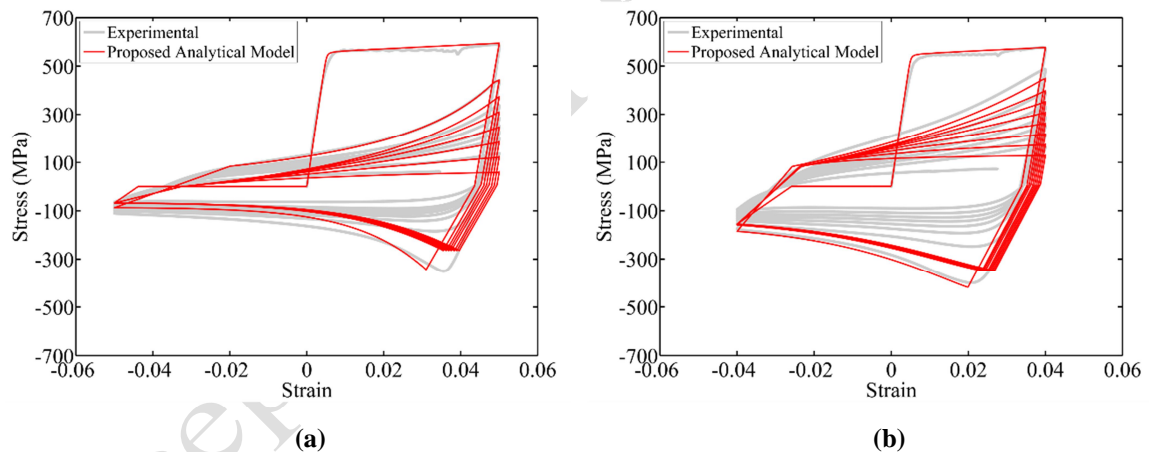
364  
365 **Fig. 15. Influence of bar diameter on fatigue material constants: (a)  $\alpha$ , (b)  $\epsilon_f$**

## 366 5. Analytical modelling

367 In recent decades the nonlinear analysis of RC framed structures subject to seismic loading  
 368 has received a lot of attention. This has been focused on the development of the fibre element  
 369 technique [14,25,26]. In this approach the member cross section is decomposed into a number  
 370 of steel and concrete fibres at selected integration points. The material nonlinearity is  
 371 represented through a uniaxial constitutive material model of steel (tension and compression)  
 372 and concrete (confined core concrete and unconfined cover concrete). Kashani et al. [27]  
 373 have developed a new phenomenological hysteretic model for reinforcing bars that includes  
 374 the effect of inelastic buckling and low-cycle fatigue degradation. It should be noted that  
 375 buckling is a second order effect due to the geometrical nonlinearity and large deformation.  
 376 Unlike the old traditional uniaxial material models for reinforcing bars [28] this advanced  
 377 material model combines the material nonlinearity due to yielding of steel with geometrical

378 nonlinearity due to buckling and low-cycle fatigue degradation into a single material model.  
 379 This model has been validated against an extensive set of experimental and numerical  
 380 simulation data of isolated reinforcing bars [6,7,24]. However, the fatigue material constants  
 381 that were used in the model development were not calibrated to include the effect of buckling  
 382 on fatigue material constants. Therefore, the experimental data generated in this paper  
 383 improves this feature of the model to include the calibrated fatigue material constants as a  
 384 function of  $\lambda_p$ . The detailed discussion of the model development and validation is available  
 385 in [13,24]. In this section the model is only used to compare the improved analytical model  
 386 with the observed experimental data.

387 A comparison between the improved model using the calibrated fatigue material constants  
 388 (provided in Table 2) and the experimental results has been made and shown in Fig 16.



389  
 390  
 391 **Fig. 16. Comparison of the proposed analytical model and the experimental results: (a) 12mm diameter**  
 392 **bar with  $L/D = 15$  at 5% strain amplitude (b) 16mm diameter bar with  $L/D = 10$  at 4% strain amplitude**

393 With reference to Fig 16, it is evident that the analytical model is capable of predicting the  
 394 complex nonlinear behaviour of the reinforcing bars. It is also evident that the prediction of  
 395 low-cycle fatigue degradation of reinforcing bars using the analytical model is in a good  
 396 agreement with experimental results.

397 This is a very important contribution and improvement to the new material model developed  
 398 by Kashani et al. [27]. The traditional material models are not able to simulate the combined

399 effect of inelastic buckling, material nonlinearity and low-cycle fatigue degradation.  
400 Therefore, using the old material models in the seismic assessment and vulnerability analysis  
401 of existing RC structures the seismic damage might be underestimated. Moreover, this  
402 material model has already been implemented into the OpenSees. Therefore, it is readily  
403 available for earthquake engineering community to be used in nonlinear seismic assessment  
404 of RC bridges/structures.

## 405 **6. Conclusions**

406 A total of ninety constant amplitude low-cycle fatigue tests are conducted. The test  
407 specimens were varied in lengths, diameter and surface condition (ribbed and smooth). Using  
408 SEM technology the fractography of fractured surface is studied. The experimental data are  
409 used to develop a new set of low-cycle fatigue model as a function of slenderness ratio and  
410 yield strength of reinforcing bars. Finally, these empirical models implemented in to a new  
411 phenomenological hysteretic model to simulate the nonlinear cyclic behaviour of reinforcing  
412 bars.

413 The main outcomes of this study can be summarised as follows:

- 414 1) The inelastic buckling has a significant impact of the cyclic stress-strain behaviour of  
415 reinforcing bars. As the buckling length of bars increased the low-cycle fatigue life  
416 decreased and therefore, the energy dissipation capacity of the bars under cyclic loading  
417 reduced.
- 418 2) The second order effect due to buckling increases the total strain amplitude at the internal  
419 face of the buckled bars. Therefore, the low-cycle fatigue cracks initiates at the internal  
420 face of the buckled bars and propagated through the bar.

- 421 3) The low-cycle fatigue tests showed that 16mm diameter bars have fractured earlier than  
422 12mm diameter bars. Therefore, the bar diameter might influence the low-cycle fatigue  
423 life of reinforcing bars. This is a very important finding and is an area for future research.
- 424 4) As expected, the ribbed bars show a less ductile failure mechanism compare to smooth  
425 bars. However, as the buckling length of bars increases the influence of ribs reduces and  
426 fracture of bars is mainly governed by the stress concentration at the internal face of  
427 buckled bars which is due to the second order effect.
- 428 5) The results of SEM analysis showed that the fractured surface of smooth bars are much  
429 darker than ribbed bars. This indicates that the crack propagation process takes much  
430 longer than ribbed bars and therefore the fracture is more ductile.
- 431 6) The new low-cycle fatigue models have been implemented into a new phenomenological  
432 hysteretic model that simulates the cyclic stress-strain behaviour reinforcing bars. The  
433 model combines the geometrical nonlinearity due to inelastic buckling, material  
434 nonlinearity due to steel yielding together and low-cycle fatigue degradation in a single  
435 uniaxial material model. This advanced material model has been implemented into the  
436 OpenSees and is readily available to the earthquake engineering community to be used in  
437 nonlinear seismic analysis of RC bridges/structures.

#### 438 **Acknowledgements**

439 The experimental work is funded by the Earthquake Engineering Research Centre (EERC) at  
440 the University of Bristol. The first author would like to thank Dr Nicholas Alexander of the  
441 University of Bristol for providing valuable guidance during the course of this research. Any  
442 findings, opinions and recommendations provided in this paper are only based on the author's  
443 view.

444



445 **References**

- 446 [1] El-Bahy A, Kunnath S.K, Stone WC, Taylor AW. Cumulative Seismic Damage of  
447 Circular Bridge Columns: Benchmark and Low-Cycle Fatigue Tests. ACI Struct J 1999;  
448 96 (4): 633-643.
- 449 [2] Lehman DE, Moehle JP. Seismic performance of well-confined concrete columns. PEER  
450 Research Report 2000; University of California at Berkeley.
- 451 [3] Brown J, Kunnath Sk. Low cycle fatigue behavior of longitudinal reinforcement in  
452 reinforced concrete bridge columns. Technical Report MCEER-00-0007; 2000.
- 453 [4] Bae S, Miseses A and Bayrak O. Inelastic buckling of reinforcing bars. J Struct Eng 2005;  
454 131 (2): 314–321.
- 455 [5] Kunnath SK, Heo Y and Mohle JF. Nonlinear uniaxial material model for reinforcing  
456 steel bars. J Struct Eng 2009; 135 (4): 335-343.
- 457 [6] Kashani MM, Crewe AJ, Alexander NA. Nonlinear stress-strain behaviour of corrosion-  
458 damaged reinforcing bars including inelastic buckling. Eng Struct 2013; 48: 417–429.
- 459 [7] Kashani MM, Crewe AJ, Alexander NA. Nonlinear cyclic response of corrosion-  
460 damaged reinforcing bars with the effect of buckling. Constr Build Mater 2013; 41: 388-  
461 400.
- 462 [8] Monti G, and Nuti C. Nonlinear cyclic behavior of reinforcing bars including buckling. J  
463 Struct Eng 1992; 118 (12): 3268–3284.
- 464 [9] Rodriguez ME, Botero JC and Villa J. Cyclic stress-strain behavior of reinforcing steel  
465 including the effect of buckling. J Struct Eng 1999; 125 (6): 605–612.
- 466 [10] Gomes A and Appleton J. Nonlinear cyclic stress-strain relationship of reinforcing bars  
467 including buckling. Eng Struct 1997; 19: 822–826.

- 468 [11] Dhakal R and Maekawa K. Modeling for postyield buckling of reinforcement. *J Struct*  
469 *Eng* 2002; 128 (9): 1139–1147.
- 470 [12] Dhakal R and Maekawa K. Path-dependent cyclic stress-strain relationship of reinforcing  
471 bar including buckling. *Eng Struct* 2002; 24: 1139–1147.
- 472 [13] Kashani MM. Seismic Performance of Corroded RC Bridge Piers: Development of a  
473 Multi-Mechanical Nonlinear Fibre Beam-Column Model, PhD Thesis 2014; University  
474 of Bristol.
- 475 [14] OpenSees, the Open System for Earthquake Engineering Simulation. (2011), PEER  
476 2011; University of California, Berkeley.
- 477 [15] BS 4449-2005 +A2. Steel for the reinforcement of concrete - Weldable reinforcing steel  
478 - bar, coil and decoiled product – Specification; 2009.
- 479 [16] Mander JB, Panthaki FD, Kasalanati A. Low-cycle fatigue behavior of reinforcing steel.  
480 *J Mater Civil Eng* 1994; 6 (4): 453-468.
- 481 [17] Brown J, Kunnath Sk. Low-cycle fatigue failure of reinforcing steel bars. *ACI Mater J*  
482 2004; 101 (6): 457-466.
- 483 [18] Higai T, Nakamura H and Saito S. Fatigue failure criterion for deformed bars subjected  
484 to large deformation reversals. *ACI SP 237-4* 2006; 237: 37-54.
- 485 [19] Hawileh RA, Abdalla JA, Oudah F and Abdelrahman K. Low-cycle fatigue life  
486 behaviour of BS 460B and BS B500B steel reinforcing bars. *Fatigue Fract Eng M* 2010;  
487 33: 397-407. (39).
- 488 [20] Manson SS. Fatigue: A complex subject-Some simple approximations. *Exp. Mech.* 1965;  
489 5 (7): 193–226.
- 490 [21] Koh SK, Stephens RI. Mean Stress Effects on Low Cycle Fatigue for a High Strength  
491 Steel. *Fat Fract Eng Materi Struct* 1991; 14 (4): 413-428.

492 [22] Chang GA, Mander JB. Seismic energy based fatigue damage analysis of bridge  
493 columns: Part I – Evaluation of seismic capacity. Technical report NCEER-94-0006,  
494 1994.

495 [23] Miner MA. Cumulative damage in fatigue. J Appl Mech 1945; 12: A159–A164.

496 [24] Kashani MM, Lowes LN, Crewe AJ, Alexander NA. Finite element investigation of the  
497 influence of corrosion pattern on inelastic buckling and cyclic response of corroded  
498 reinforcing bars. Eng Struct 2014; 75: 113-125.

499 [25] Spacone E, Filippou FC and Taucer FF. Fibre beam-column model for non-linear  
500 analysis of r/c frames: part I: formulation. Earthq Eng Struct D 1996; 25: 711-725.

501 [26] Spacone E, Filippou FC and Taucer ff. Fibre beam-column model for non-linear analysis  
502 of R/C frames: part II: applications. Earthq Eng Struct D 1996; 25: 727-742.

503 [27] Kashani MM, Lowes LN, Crewe AJ, Alexander NA. Phenomenological hysteretic model  
504 for corroded reinforcing bars including inelastic buckling and low-cycle fatigue  
505 degradation. Comp & Struct 2015; 156: 58-71.

506 [28] Menegotto M, and Pinto PE. Method of analysis of cyclically loaded RC plane frames  
507 including changes in geometry and nonelastic behavior of elements under normal force  
508 and bending. Preliminary Report IABSE, Zurich 1973; 13: 15–22.

509

510

511

512

513

514

515

516 **Appendix A. Low-cycle fatigue test results**

517 **Table A1. Low-cycle fatigue test results of 12mm diameter ribbed bars**

<i>L/D</i>	Total Time (s)	Frequency (Hz)	Number of Half Cycles to Failure ( $2N_f$ )	Total Normalised Dissipated Energy ( $E_t/E_y$ )
<b>1% Strain Amplitude</b>				
5	3733.14	0.125	933	2835
8	1333.62	0.125	333	1489
10	887.13	0.125	222	1021
12	591.36	0.125	148	523
15	576.23	0.125	144	382
<b>1.5% Strain Amplitude</b>				
5	1991.08	0.083	332	2566
8	765.87	0.083	128	1120
10	596.83	0.083	99	613
12	488.72	0.083	81	398
15	428.51	0.083	71	294
<b>2% Strain Amplitude</b>				
5	1124.69	0.063	141	1831
8	506.56	0.063	63	649
10	409.95	0.063	51	429
12	361.01	0.063	45	312
15	426.05	0.063	53	267
<b>3% Strain Amplitude</b>				
5	607.52	0.042	51	1245
8	348.84	0.042	29	464
10	298.79	0.042	25	310
12	441.57	0.042	37	349
15	393.49	0.042	33	244
<b>4% Strain Amplitude</b>				
5	527.26	0.031	33	1094
8	366.02	0.031	23	458
10	267.21	0.031	17	289
12	425.70	0.031	27	314
15	363.16	0.031	23	231
<b>5% Strain Amplitude</b>				
5	402.91	0.025	20	846
8	328.22	0.025	16	414
10	328.61	0.025	16	303
12	323.06	0.025	16	246
15	330.17	0.025	17	220

518  
519  
520  
521  
522

Table A2. Low-cycle fatigue test results of 16mm diameter ribbed bars

<i>L/D</i>	Total Time (s)	Frequency (Hz)	Number of Half Cycles to Failure ( $2N_f$ )	Total Normalised Dissipated Energy ( $E_t/E_y$ )
<b>1% Strain Amplitude</b>				
5	4870.26	0.125	1218	3328
8	1364.69	0.125	341	1457
10	734.32	0.125	184	867
12	543.52	0.125	136	579
15	494.98	0.125	124	370
<b>1.5% Strain Amplitude</b>				
5	1937.77	0.083	323	2389
8	677.83	0.083	113	993
10	393.67	0.083	66	500
12	379.64	0.083	63	355
15	365.60	0.083	61	267
<b>2% Strain Amplitude</b>				
5	1050.74	0.063	131	1677
8	358.74	0.063	45	548
10	343.91	0.063	43	397
12	391.40	0.063	49	366
15	295.94	0.063	37	226
<b>2.5% Strain Amplitude</b>				
5	628.92	0.050	63	1205
8	289.43	0.050	29	438
10	267.66	0.050	27	318
12	265.82	0.050	27	258
15	312.27	0.050	31	231
<b>3% Strain Amplitude</b>				
5	558.47	0.042	47	1147
8	248.10	0.042	21	378
10	268.79	0.042	22	318
12	249.61	0.042	21	240
15	298.71	0.042	25	216
<b>4% Strain Amplitude</b>				
5	420.98	0.031	26	959
8	203.31	0.031	13	340
10	230.94	0.031	14	268
12	267.05	0.031	17	244
15	290.12	0.031	18	213

524  
525  
526  
527  
528  
529  
530  
531

Table A3. Low-cycle fatigue test results of 12mm diameter smooth bars

<i>L/D</i>	Total Time (s)	Frequency (Hz)	Number of Half Cycles to Failure ( $2N_f$ )	Total Normalised Dissipated Energy ( $E_t/E_y$ )
<b>1% Strain Amplitude</b>				
5	10168	0.125	2452	5603
8	0.00	0.125	0	0
10	1944.38	0.125	486	1861
12	1530.27	0.125	383	1066
15	1117.62	0.125	279	604
<b>1.5% Strain Amplitude</b>				
5	4404	0.083	734	5603
8	1375.75	0.083	229	1500
10	1194.59	0.083	199	894
12	1120.97	0.083	187	679
15	1013.16	0.083	169	486
<b>2% Strain Amplitude</b>				
5	2937.79	0.063	367	4289
8	1096.16	0.063	137	997
10	1012.93	0.063	127	691
12	916.97	0.063	115	518
15	828.23	0.063	104	380
<b>3% Strain Amplitude</b>				
5	1659.46	0.042	138	2378
8	894.38	0.042	75	707
10	871.71	0.042	73	548
12	755.93	0.042	63	402
15	772.20	0.042	64	334
<b>4% Strain Amplitude</b>				
5	1287.05	0.031	80	1664
8	742.60	0.031	46	591
10	710.24	0.031	44	456
12	709.25	0.031	44	378
15	772.80	0.031	48	319
<b>5% Strain Amplitude</b>				
5	1018.59	0.025	51	1284
8	687.06	0.025	34	544
10	685.54	0.025	34	428
12	685.24	0.025	34	355
15	693.35	0.025	35	296